Characterization of Embedded Passives Using Macromodels in LTCC Technology

Kwang Lim Choi, Nanju Na, and Madhavan Swaminathan, *Member, IEEE*

***Abstract*— This paper discusses the frequency and time domain response of embedded passive components in a multilayered structure fabricated using low temperature co-fired ceramic (LTCC) technology. A rational polynomial approximation that combines the accuracy of EM solvers with interpolation methods has been used to capture the frequency dependent losses and parasitics of embedded passives in a macro-model. This method allows for a significant speed-up in computation time while using commercial EM solvers. The macromodel with suitable modification has been used to compute the time domain response in SPICE for typical embedded passive structures. Simulation results show good correlation with time domain reflectometry/time-domain-transmission (TDR/TDT) measurements. The behavior of embedded passives in the high frequency operation of transmission lines and voltage divider networks has also been discussed.**

***Index Terms*— Embedded passives, interpolation technique, macromodeling, multilayered packaging, portable wireless.**

I. Introduction

THE trend in portable wireless electronics is to combine digital and RF circuits into a compact packaged mixed signal module. Examples of such electronics are pagers, cellular phones, transceivers, and global positioning systems that typically function in the frequency range DC–5 GHz. Embedded passives which is an emerging technology area provides a method for achieving size shrinkage by replacing surface mount components with embedded components in a multilayered packaging environment. The embedded components, however, have different electrical characteristics as compared to discrete components due to their geometric structure and parasitic effects. Therefore, these effects should be characterized and carefully considered in mixed signal wireless applications.

Three critical parameters are often used to design embedded passive components (resistors, inductors, and capacitors) in RF circuits namely, variation of resistance/reactance with frequency, variation of quality factor (Q) with frequency and the resonance behavior of the component. Numerous methods are available to analyze these structures such as partial element equivalent circuit (PEEC) [1] approach, empirical techniques and full wave electromagnetic (EM) methods (SONNET [2], HFSS [3]) to name a few. Since the accuracy of the response over a large bandwidth is critical in designing high frequency circuits, the appropriate method has to be applied for the analysis [4]. Numerical techniques such as method of moments, finite element, finite difference time domain (FDTD) which discretize Maxwell's equations with the appropriate boundary conditions provide the accuracy necessary over a large bandwidth for most structures.

As an example, the results from SONNET [2], a method of moments based EM solver that discretizes the integral form of Maxwell's equation, have been compared with measured results for a one-port RF spiral inductor fabricated using low temperature cofired ceramic technology (LTCC), as shown in Fig. 1. Fig. 1(a) shows the physical details of the spiral inductor, while Fig. 1(b) and (c) show the variation of the reactance and quality factor (Q) with frequency. In the figure, the reactance is the imaginary part of the complex input impedance while the quality factor is the ratio of the imaginary to the real part of the input impedance. As can be seen from the figure, the agreement between SONNET and measurements is fairly good (˜15% error).

Based on Fig. 1(b) and (c), two important features that are typical and characteristic of embedded passives can be extracted, namely

1) The frequency variation of the reactance which produces resonance is caused by the parasitics associated with the structure. For example, for the spiral inductor, the parasitic is the capacitance within the spiral and between the spiral and the ground plane.
2) The variation of the Q-factor, which is a measure of the loss in the structure, is a result of the DC resistance, current crowding, and skin effect (variation of resistance with frequency), coupled with the parasitics. The responses in Fig. 1(b) and (c) are critical for the design of high frequency circuits.

For all the embedded passive components considered in this paper, SONNET provided good results in the frequency range DC–20 GHz and hence has been used throughout this paper. The problem with most three-dimensional (3-D) EM solvers is the large analysis time required which could be of the order of hours for simple structures [4]. Moreover, when these embedded passives are used as part of a digital circuit, a method is necessary that allows the use of frequency dependent models in a time domain simulation. An example is the use of embedded resistors for terminating digital transmission lines. Though SONNET has been used here to obtain the frequency data, any EM solver that computes the accurate frequency domain response can be used. This paper assumes that an EM

Manuscript received January 1, 1998; revised May 23, 1998. This work was supported in part by Defense Advanced Research Project Agency (DARPA) through Sarnoff Corporation under Contract F33615-96-2-5105, and also by the Packaging Research Center under Contract EEC9402723.

The authors are with the School of Electrical and Computer Engineering, Packaging Research Center, Georgia Institute of Technology, Atlanta, GA 30332-0250 USA (e-mail: madhavan.swaminathan@ece.gatech.edu).

Publisher Item Identifier S 1070-9894(98)06065-4.

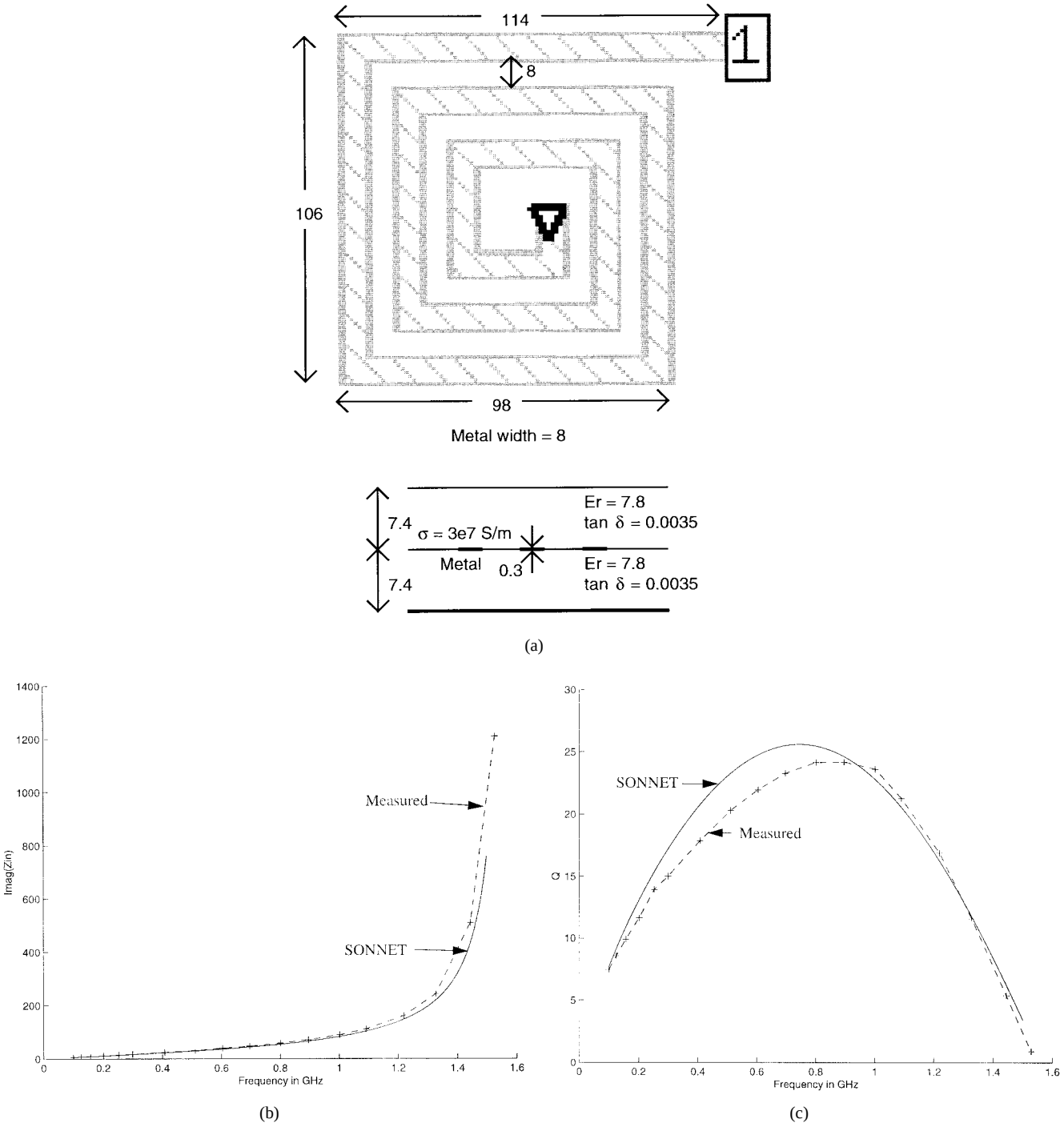

Fig. 1. (a) The inductor structure. All units are in mils, (b) reactance of the inductor in Ω, and (c) Q of the inductor.

solver capable of handling 3-D embedded passive structures is available.

Given these issues, the objectives of this paper are as follows.

1) Extraction of the frequency response of embedded passives over the desired bandwidth using interpolation techniques. This results in a considerable speed-up for EM computation by reducing the number of points required to generate the frequency domain response. Cauchy's method which is an interpolation technique using rational polynomials has been used here to meet this objective [4]. This method has been used in the past for scattering problems [5], [6] and has been applied here for embedded passive structures. Though Cauchy's method has been discussed at length in [5], [6], the purpose of including it in this paper is to enable speed-up in computation time as well as to enable the appropriate modification of the rational polynomial for transient simulation.
2) Modification of the rational polynomial in 1) to enable time-domain simulation that includes frequency dependent losses and parasitics. This represents the major

contribution of this paper which has not been discussed in [5], [6]. Since a transient waveform has real values, the rational polynomial in 1) has to be suitably modified to include complex conjugate poles and zeros. This is an additional constraint that has to be imposed while generating the rational polynomial. Since the response of the passive has been captured using a rational polynomial, as opposed to an equivalent circuit, the resulting model has been called a macromodel.

Time domain reflectometry (TDR) and time domain transmission (TDT) measurements have been used in this paper to confirm the results of the macromodel. The authors believe that an important contribution of this paper is the correlation between macromodels and the measured time domain responses of the embedded passive structures.

II. Interpolation Using Cauchy's Method for Embedded Passives

Consider a function in the frequency domain which can be represented as

$$H(s) = \frac{\sum_{k=0}^{P} a_k \cdot s^k}{\sum_{l=0}^{Q} b_l \cdot s^l} \tag{1}$$

where $s = j\omega$, ω is the angular frequency and a_k and b_l are complex coefficients. Function $H(s)$ could either be impedance, admittance or scattering parameters. Equation (1) can be rewritten as

$$\sum_{k=0}^{P} a_k \cdot s^k - H(s) \cdot \sum_{l=0}^{Q} b_l \cdot s^l = 0 \tag{2}$$

which can be represented in a matrix form [1]

$$[A][x] = 0 \tag{3}$$

where [A] is shown in (4), at the bottom of the page, and $[x]$ is a solution vector that contains all the coefficients of $H(s)$ as

$$[x] = [a_0\ a_1\ \cdots\ a_P\ b_0\ b_1\ \cdots\ b_Q]^T. \tag{5}$$

The variable "m" is the number of available data points with $m \geq P+Q+2$ where P and Q are the orders of the numerator and denominator, respectively, in (1). The nonzero singular values of the $[A]$ matrix in (4) determine the rank of the matrix and could be used to obtain an estimate for P and Q, as discussed in [2]. In general, the order of the polynomials in (1) is chosen such that $Q = P+1$ although it is not a required condition. The data points need not be equally spaced in frequency. The usefulness of setting up the matrix equation as in (3) is the nonrequirement for the derivatives of the function $H(s)$ at a given frequency point using Taylor series expansion [3]. Since (3) is generated through a set of partial data points and do not involve any derivatives, the equation can be readily applied to compute the response of passive components using commercial EM solvers. Once the orders, P and Q, of the polynomials are determined, the coefficients, a_k and b_l, can be computed by solving

$$[A]^H[A][x] = 0 \tag{6}$$

where $[x]$ is found by solving the eigenvector corresponding to the minimum eigenvalue [2] of $[A]^H[A]$ in (6). The superscript "H" denotes the complex conjugate transpose of the matrix $[A]$. Since no condition is enforced on the coefficients, a_k and b_l, and since the matrix $[A]^H[A]$ is complex, the eigenvectors are complex. Hence the coefficients, a_k and b_l, are complex. Equation (6), however, allows one to interpolate the response by determining the coefficients, a_k and b_l, once the order of the polynomial (P and Q) is determined. The objective of (6) is, therefore, to determine the minimum values of P and Q and the corresponding coefficients, a_k and b_l, such that the error in the computed response is within a threshold value. Min$\{P, Q\}$ can be determined by starting with a large initial value for P and Q (say $P = 10$ and $Q = 11$), checking the singular values of the matrix $[A]^H[A]$, relating it to the rank of the matrix [2] and suitably modifying P and Q.

As an example of the application of (6), Fig. 2 shows the simulated response of the inductor shown in Fig. 1(a) and the results of the polynomials generated using the interpolation method. SONNET was first used to solve for the input impedance by suitably discretizing the physical structure and computing the response at enough frequency points to capture the behavior. This required the solution at 24 equally spaced

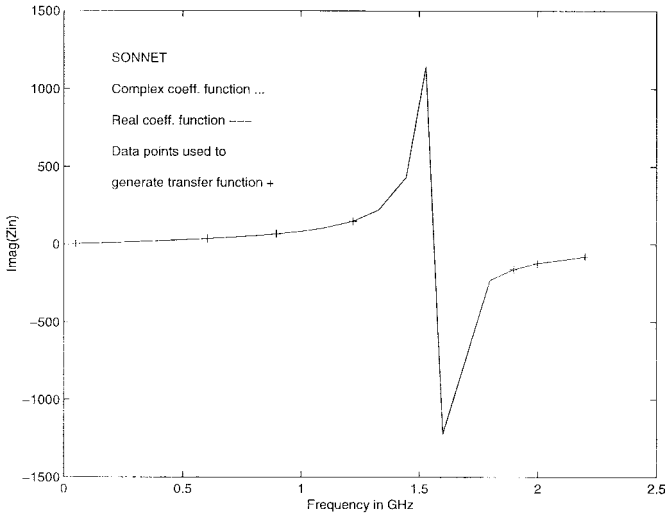

Fig. 2. Reactance of the inductor in Ω.

$$[A] = \begin{bmatrix} (s_1)^0 & (s_1)^1 & \cdots & (s_1)^P & -H(s_1)\cdot(s_1)^0 & -H(s_1)\cdot(s_1)^1 & \cdots & -H(s_1)^Q \\ (s_2)^0 & (s_2)^1 & \cdots & (s_2)^P & -H(s_2)\cdot(s_2)^0 & -H(s_2)\cdot(s_2)^1 & \cdots & -H(s_2)^Q \\ \vdots & \vdots & \vdots & \vdots & \vdots & \vdots & \vdots & \vdots \\ (s_m)^0 & (s_m)^1 & \cdots & (s_m)^P & -H(s_m)\cdot(s_m)^0 & -H(s_m)\cdot(s_m)^1 & \cdots & -H(s_m)^Q \end{bmatrix} \tag{4}$$

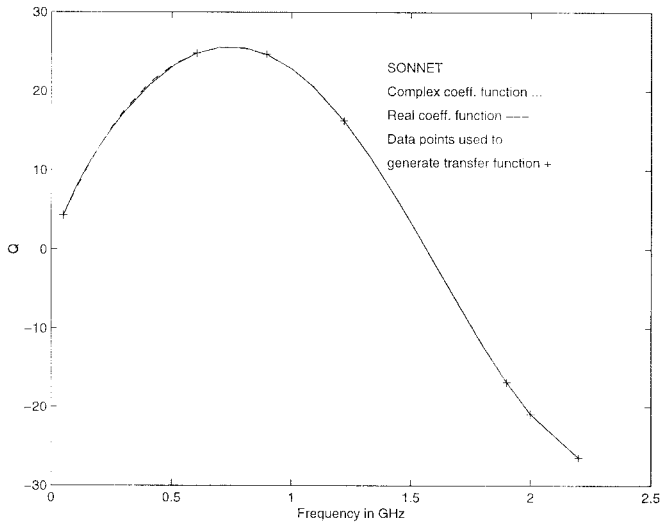

Fig. 3. Q of the inductor.

frequency points in the frequency range DC–2.2 GHz, since the resonant frequency was not known *a priori*. Next, the interpolation algorithm was applied. Based on initial analysis using the singular values of the matrix $[A]^H[A]$, a value of $P = 2$ and $Q = 3$ was determined and found to produce acceptable response for spiral inductors. This translated to a requirement for seven data points ($P + Q$+2) to capture the response in the frequency range DC–2.2 GHz. SONNET was used to compute the input impedance at seven arbitrarily chosen frequency points as shown in Figs. 2 and 3 where the response obtained from (7) in the frequency range DC–2.2 GHz has been overlaid in Figs. 2 and 3. The tic (+) marks indicate the data samples used for interpolation. As can be seen from the figures, (7) captured the resonant frequency very accurately even though no data point was chosen at the resonant frequency. The error between SONNET (solved with 24 frequency points) and the interpolated response using (7) is shown in Fig. 4 with the largest error being <3%, showing the accuracy of the method. The interpolation algorithm resulted in a rational polynomial of the normalized Z_{in} with frequency scaling factor of 10^{10} as

$$Z_{\text{in}}(s) = \frac{a_0 + a_1 \cdot s + a_2 \cdot s^2}{b_0 + b_1 \cdot s + b_2 \cdot s^2 + b_3 \cdot s^3}$$

$$\begin{aligned} a_0 &= -6 \cdot 10^{-4} + 0.0128i \\ a_1 &= 0.6496 + 0.7505i \\ a_2 &= -0.0822 + 0.4585i \\ b_0 &= 0.407 + 0.4654i \\ b_1 &= -0.0624 + 0.3481i \\ b_2 &= 0.1842 + 0.4741i \\ b_3 &= -0.0627 + 0.1093i. \end{aligned} \tag{7}$$

To ensure that the frequency response could be interpolated using a small number of data points for similar classes of structures, the response of the spiral inductor was extracted using the interpolation algorithm for varying physical parameters. The interpolation algorithm used six equally spaced data points (by restricting $a_0 = 1$) over 4 GHz bandwidth and its

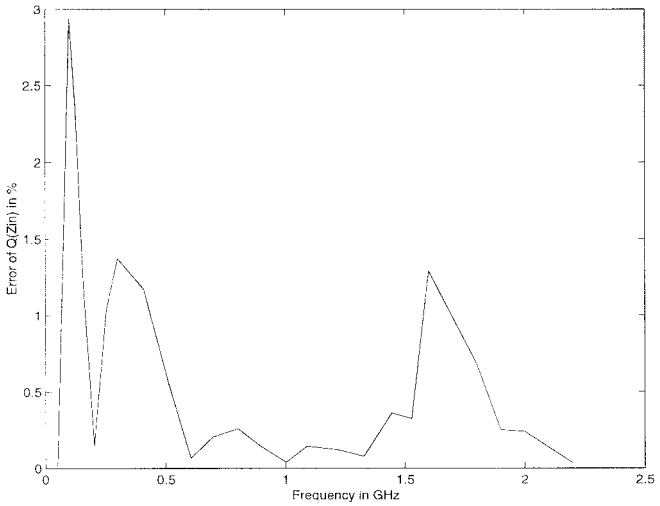

(a)

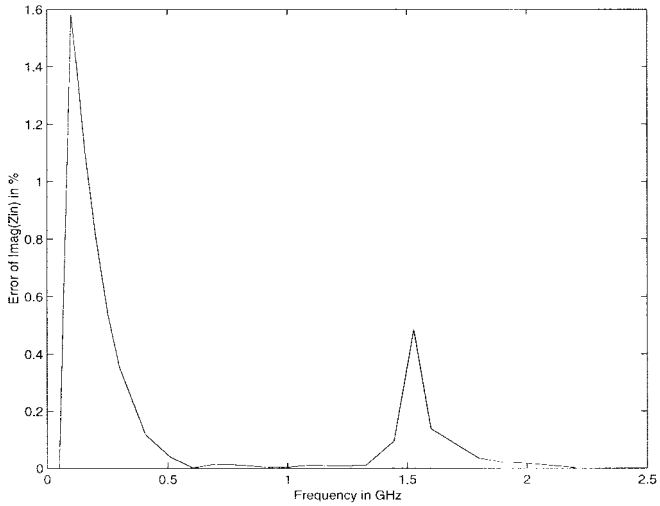

(b)

Fig. 4. Error of (a) Imag(Z_{in}) and (b) Q of Z_{in} in %.

result has been compared to the frequency response obtained using 40 data points equally spaced with 100 MHz interval. The error between the actual response and the interpolated response is shown in Fig. 5 where the error bound is less than 6%.

Table I compares the simulation time required with and without the interpolation method [5]. Details of the embedded capacitor in Table I are discussed later in this paper. As can be seen from Table I, the interpolation technique is useful for complicated multilayered structures such as capacitors and provides a means for significant speed-up in computation time.

III. Developing Macromocels in SPICE

As mentioned earlier, one of the objectives of this paper is to enable a time domain simulation using the rational polynomial approximation. This is possible through a discrete convolution between the transfer function in (1) and the input pulse, as discussed in [7]. To enable a time domain simulation, the coefficients, a_k and b_l, in (1) must be real. This results in complex conjugate and real poles which are translated into

TABLE I
COMPARISON OF SIMULATION TIME REQUIRED WITH AND WITHOUT THE INTERPOLATION METHOD

		SONNET		Present Method	
Type	Frequency Band	Data Points	Simulation Time	Data Points	Simulation Time
Inductor	DC - 2.2 GHz	24	15.2 minutes	7	4.4 minutes
Capacitor	DC - 4 GHz	40	3.7 hours	7	39 minutes

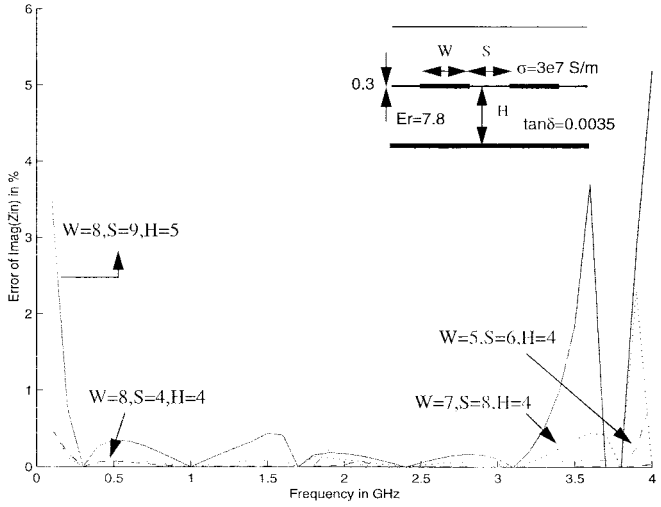

(a)

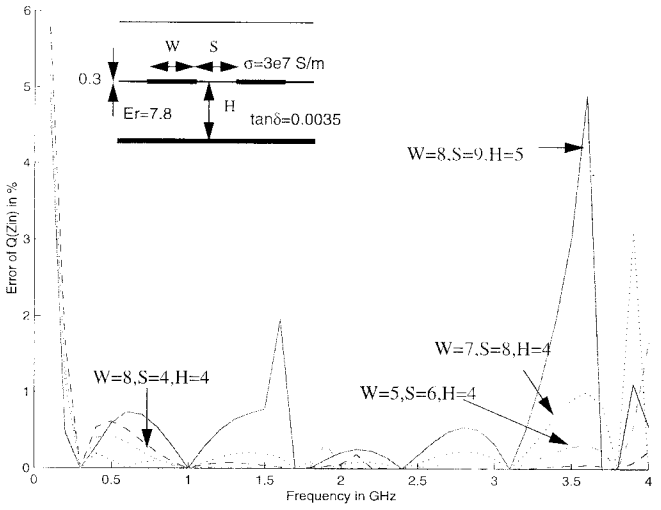

(b)

Fig. 5. Error of (a) Imag(Z_{in}) and (b) Q for varying W, H, S for spiral inductor.

sine, cosine, and exponential functions during convolution. Another requirement is stability through passivity by ensuring that all the poles are on the left half plane (LHP) [8].

Real coefficients, a_k and b_l, in (2) can be obtained by enforcing the condition that the coefficients, a_k and b_l, are real in (1). This is possible by modifying (2) to the form

$$\sum_{k=0}^{P} a_k \cdot \text{Re}(s^k) - \sum_{l=0}^{Q} b_1 \cdot \text{Re}(H(s) \cdot s^l) = 0 \qquad (8a)$$

$$\sum_{k=0}^{P} a_k \cdot \text{Im}(s^k) - \sum_{l=0}^{Q} b_l \cdot \text{Im}(H(s) \cdot s^l) = 0 \qquad (8b)$$

and solving the eigenvalue equation

$$[A]^H[A][x] = \lambda_{\min}[x] \qquad (9)$$

where the matrix elements in (9) are from (8). In (9), "$\lambda_{\min}$" is the minimum eigenvalue and $[x]$ is the corresponding eigenvector with real elements.

To develop rational polynomials with real coefficients, it is important to note that higher order polynomials are required as compared to complex coefficient polynomials. Therefore, solving for a higher order polynomial further requires more data points which translates to more simulation time if directly coupled to an EM solver such as SONNET. To minimize the number of data points and hence minimize the analysis time to obtain a suitable polynomial representation, interpolation is first performed by computing the complex coefficient function which can then provide the required number of data points to solve for the real coefficient function. Once the complex coefficient function is found, a larger matrix $[A]$ in (4) is recreated with higher P, Q, and "m" from the complex coefficient function. Our experience based on the classes of structures considered in this paper has been that the order of P and Q for real coefficients is one more than that required for complex coefficients. For example, for the spiral inductor, $P = 3$ and $Q = 4$ in (8).

All the discussions so far have been based on the assumption that the structure is a one-port circuit. The equation and analysis technique can be readily extended to two-ports or other multiple-port circuits. An example of a two-port circuit is the admittance parameters y_{11}, y_{12}, y_{21}, and y_{22} for an embedded resistor. This can be represented in equation form as

$$\begin{pmatrix} I_1 \\ I_2 \end{pmatrix} = \begin{pmatrix} y_{11} & y_{12} \\ y_{21} & y_{22} \end{pmatrix} \cdot \begin{pmatrix} V_1 \\ V_2 \end{pmatrix} \qquad (10)$$

where

$$y_{11} = \frac{\sum_{k=0}^{P_1} a_{1,k} \cdot s^k}{\sum_{l=0}^{Q} b_l \cdot s^l} \quad y_{21} = y_{12} = \frac{\sum_{k=0}^{P_2} a_{2,k} \cdot s^k}{\sum_{l=0}^{Q} b_l \cdot s^l}$$

$$y_{22} = \frac{\sum_{k=0}^{P_3} a_{3,k} \cdot s^k}{\sum_{l=0}^{Q} b_l \cdot s^l}. \qquad (11)$$

In (11), the admittance parameters have a common denominator and hence the same poles. The coefficients, $a_{n,k}$ and b_l

are obtained by solving (9) where $[A]$ is, as shown in (12) at the bottom of the page, and "n" is the number of parameters to be solved for a common denominator. In the case of 2-port embedded resistor, the value of "n" is 3 and the transfer functions, H_1, H_2, and H_3, correspond to y_{11}, y_{21}, and y_{22}, respectively. In general, the numerator orders, P_1, P_2, and P_3 are the same for all parameters although our experience shows that it is not a required condition [see (12)]. The solution vector $[x]$ contains the numerator coefficients, $a_{n,k}$, for each parameter along with the common denominator coefficients, b_l, as

$$[x] = [a_{1,1}\ a_{1,2}\ \cdots\ a_{1,m}\ :\ a_{2,1}\ a_{2,2}\ \cdots\ a_{2,m}\ :\ \cdots\ :\ a_{n,1}\ a_{n,2}\ \cdots\ a_{n,m}\ :\ b_1\ b_2\ \cdots\ b_m]^T. \tag{13}$$

It should be noted that it is not necessary to compute the solution of complex coefficients before computing the solution of real coefficients as presented in this section. The values of P and Q found by singular value decomposition [6] are the minimum polynomial orders required to approximate a complex coefficient function using the minimum number of data points, $P+Q+2$. When the number of available data from EM solver is much larger than $P+Q+2$, the larger matrix $[A]$ in (4) for one-port structure or the matrix $[A]$ in (12) for multiple-port structure can be directly created from EM generated data, bypassing computation of complex coefficient solution. However, this is done at a cost of more EM simulation time.

IV. Algorithm for Developing Macromodels

Step 1) For a typical passive structure (say spiral inductor), generate a set of data points over the bandwidth of interest by assuming a large value for P and Q (say $P = 10$ and $Q = 11$). This step is necessary to determine the order of the complex coefficient polynomials and is done only once for a class of structures. Solve (6) to determine minimum P and Q by checking the singular values of matrix $[A]^H[A]$.

Step 2) Results of Step 1 determine the number of frequency points required in the future for similar structures. The number of frequency points is equal to $P+Q+2$ where the frequency points span the band of interest. Based on the RF structures analyzed over the frequency band DC–4 GHz in this paper, the order of the polynomials (complex coefficients) required were typically $P = 2$ and $Q = 3$.

Step 3) Solve (6) to compute complex coefficients, a_k and b_l.

Step 4) Generate the complex coefficient function $H(s)$ using (1) and compute poles and zeros as appropriate.

Step 5) If the structure has only 1-port, reconstruct the matrix in (4) with higher P and Q from complex coefficient function based on (8). Solve (9) to compute real coefficients, a_k and b_l.

Step 6) If the structure has multiple ports, a matrix in (12) is created from complex coefficient function of each parameter. Solve (9) to compute real coefficients which has the common denominator as well as numerator coefficients for each parameter.

V. Stability

As mentioned earlier, SPICE macromodels require left half plane (LHP) poles to ensure passivity. As is well known, increasing the order of the polynomial does not guarantee LHP poles, nor does it guarantee a better solution. In the past, AWE

$$[A] = \begin{bmatrix}
\mathrm{Re}(s_{1,1}^{0}) & \cdots & \mathrm{Re}(s_{1,1}^{P_1}) & & & & \mathrm{Re}(-H_1(s_{1,1})\cdot(s_{1,1}^{0})) & \cdots & \mathrm{Re}(-H_1(s_{1,1})\cdot(s_{1,1}^{Q})) \\
\vdots & \vdots & \vdots & & & & \vdots & \vdots & \vdots \\
\mathrm{Re}(s_{1,m}^{0}) & \cdots & \mathrm{Re}(s_{1,m}^{P_1}) & & & & \mathrm{Re}(-H_1(s_{1,m})\cdot(s_{1,m}^{0})) & \cdots & \mathrm{Re}(-H_1(s_{1,m})\cdot(s_{1,m}^{Q})) \\
\mathrm{Im}(s_{1,1}^{0}) & \cdots & \mathrm{Im}(s_{1,1}^{P_1}) & & & & \mathrm{Im}(-H_1(s_{1,1})\cdot(s_{1,1}^{0})) & \cdots & \mathrm{Im}(-H_1(s_{1,1})\cdot(s_{1,1}^{Q})) \\
\vdots & \vdots & \vdots & & & & \vdots & \vdots & \vdots \\
\mathrm{Im}(s_{1,m}^{0}) & \cdots & \mathrm{Im}(s_{1,m}^{P_1}) & & & & \mathrm{Im}(-H_1(s_{1,m})\cdot(s_{1,m}^{0})) & \cdots & \mathrm{Im}(-H_1(s_{1,m})\cdot(s_{1,m}^{Q})) \\
\multicolumn{3}{c}{0} & \cdots & \multicolumn{2}{c}{0} & \multicolumn{3}{c}{0} \\
\multicolumn{3}{c}{0} & \cdots & \multicolumn{2}{c}{0} & \multicolumn{3}{c}{0} \\
\mathrm{Re}(s_{2,1}^{0}) & \cdots & \mathrm{Re}(s_{2,1}^{P_2}) & & & & \mathrm{Re}(-H_2(s_{2,1})\cdot(s_{2,1}^{0})) & \cdots & \mathrm{Re}(-H_2(s_{2,1})\cdot(s_{2,1}^{Q})) \\
\vdots & \vdots & \vdots & \ddots & & \vdots & \vdots & \vdots & \vdots \\
\mathrm{Re}(s_{2,m}^{0}) & \cdots & \mathrm{Re}(s_{2,m}^{P_2}) & & & & \mathrm{Re}(-H_2(s_{2,m})\cdot(s_{2,m}^{0})) & \cdots & \mathrm{Re}(-H_2(s_{2,m})\cdot(s_{2,m}^{Q})) \\
\mathrm{Im}(s_{2,1}^{0}) & \cdots & \mathrm{Im}(s_{2,1}^{P_2}) & & & & \mathrm{Im}(-H_2(s_{2,1})\cdot(s_{2,1}^{0})) & \cdots & \mathrm{Im}(-H_2(s_{2,1})\cdot(s_{2,1}^{Q})) \\
\vdots & \vdots & \vdots & \ddots & & \vdots & \vdots & \vdots & \vdots \\
\mathrm{Im}(s_{2,m}^{0}) & \cdots & \mathrm{Im}(s_{2,m}^{P_2}) & & & & \mathrm{Im}(-H_2(s_{2,m})\cdot(s_{2,m}^{0})) & \cdots & \mathrm{Im}(-H_2(s_{2,m})\cdot(s_{2,m}^{Q})) \\
\multicolumn{3}{c}{0} & \ddots & \multicolumn{2}{c}{0} & \multicolumn{3}{c}{\vdots} \\
\mathrm{Re}(s_{n,1}^{0}) & \cdots & \mathrm{Re}(s_{n,1}^{P_n}) & & & & \mathrm{Re}(-H_n(s_{n,1})\cdot(s_{n,1}^{0})) & \cdots & \mathrm{Re}(-H_n(s_{n,1})\cdot(s_{n,1}^{Q})) \\
\vdots & \vdots & \vdots & & & & \vdots & \vdots & \vdots \\
\mathrm{Re}(s_{n,m}^{0}) & \cdots & \mathrm{Re}(s_{n,m}^{P_n}) & & & & \mathrm{Re}(-H_n(s_{n,m})\cdot(s_{n,m}^{0})) & \cdots & \mathrm{Re}(-H_n(s_{n,m})\cdot(s_{n,m}^{Q})) \\
\mathrm{Im}(s_{n,1}^{0}) & \cdots & \mathrm{Im}(s_{n,1}^{P_n}) & & & & \mathrm{Im}(-H_n(s_{n,1})\cdot(s_{n,1}^{0})) & \cdots & \mathrm{Im}(-H_n(s_{n,1})\cdot(s_{n,1}^{Q})) \\
\vdots & \vdots & \vdots & & & & \vdots & \vdots & \vdots \\
\mathrm{Im}(s_{n,m}^{0}) & \cdots & \mathrm{Im}(s_{n,m}^{P_n}) & & & & \mathrm{Im}(-H_n(s_{n,m})\cdot(s_{n,m}^{0})) & \cdots & \mathrm{Im}(-H_n(s_{n,m})\cdot(s_{n,m}^{Q}))
\end{bmatrix} \tag{12}$$

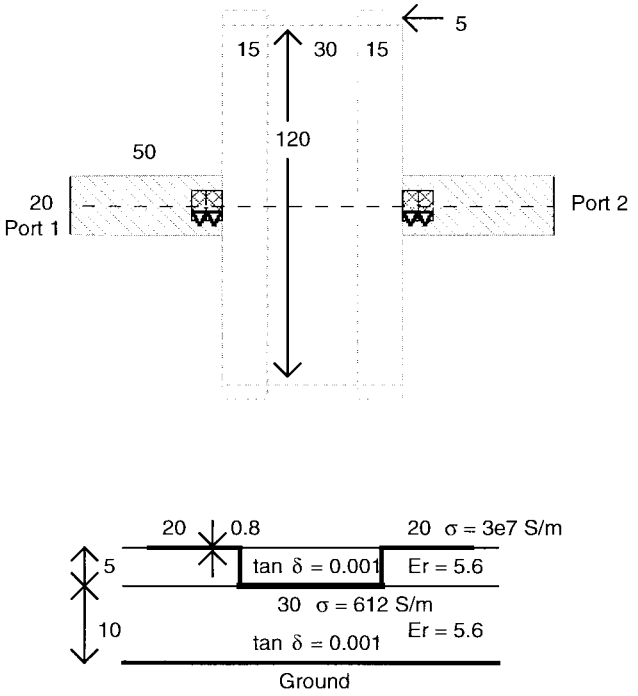

Fig. 6. Top and side view of the 26 Ω resistor structure. The units are in mils.

based techniques [7], [9] have been applied to transmission lines to obtain a rational polynomial approximation. The main element that differentiates transmission lines from embedded passives discussed in this paper are the number of poles required to produce an acceptable response. In all the cases that were considered in this paper, no more than four poles were required to develop a macromodel and create an acceptable response in the range of DC–4 GHz. For a bandwidth in the range of DC–20 GHz, no more than five poles were required. Given the small number of poles, a stable solution could always be obtained by following these guidelines:

1) The results were extremely sensitive to the frequency scaling factor which was necessary to normalize the frequency (due to powers of "s"). The optimum scaling factor was determined by checking the spread in the eigenvalues. A large spread invariably produced an unstable solution.
2) Minimizing the orders of polynomial, P and Q, was always necessary for a stable solution. If this was not the case, the result had multiple zero eigenvalues which pointed toward an unstable solution.

VI. Measurement Correlation

The SPICE macromodels were simulated in the time domain and correlated with time domain reflectometry (TDR) and time domain transmission (TDT) measurements [10], [11]. The measurement set-up consisted of Tektronix 11 801B digital sampling oscilloscope, SD-24 (20 GHz bandwidth) sampling heads with dual channels, Cascade Microtech G-S-G probes, Cascade Microtech probe station, and high frequency Gore cables. A 250 mV step with a rise-time of 35 ps was propagated on the structure and both the reflected and transmitted pulses were measured. Suitable SPICE models of the set-up

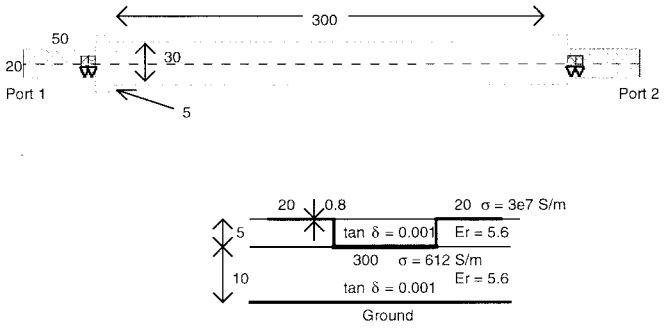

Fig. 7. Top and side view of the 858 Ω resistor structure. The units are in mils.

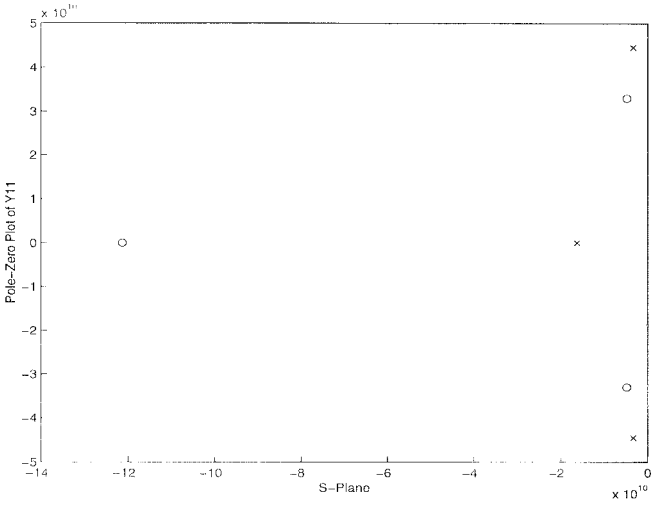

Fig. 8. Pole-zero plot of y_{11} of 26 Ω resistor.

for measurement incorporating macromodels were developed in order to correlate macromodels to measured data.

The technique was applied to two 2-port embedded resistors shown in Figs. 6 and 7. The structures were realized by LTCC Technology. In Figs. 6 and 7, metallization connecting to ports 1 and 2 provided access to the resistors through a co-planar transition. To develop SPICE macromodels for the resistors which had DC resistance of 26 and 858 Ω, the polynomial orders, $P = 2$ and $Q = 3$, were used to approximate the admittance parameters using complex coefficients while $P = 3$ and $Q = 4$ were needed to represent the same response using real coefficients. A frequency scaling factor of 10^9 was used. The pole-zero plot of the 26 Ω resistor is shown in Fig. 8 for the admittance parameter y_{11} represented using the rational polynomial. As can be seen from the figure, the poles are on the LHP. Fig. 9 shows the frequency response of the 26 Ω resistor generated by SONNET [2] and the interpolated results indicating that the agreement is very good. Table II shows the SPICE macromodel generated using the approximated admittance functions (with the inefficient values not shown).

Fig. 10 shows the measured and simulated TDR response of the 26 Ω embedded resistor. The initial negative peak represents the capacitance parasitic (between resistor and ground plane) which has been captured accurately by the macromodel. Fig. 11 shows the measured and simulated TDT response for the 858 Ω resistor. Fig. 11 consists of four waveforms namely,

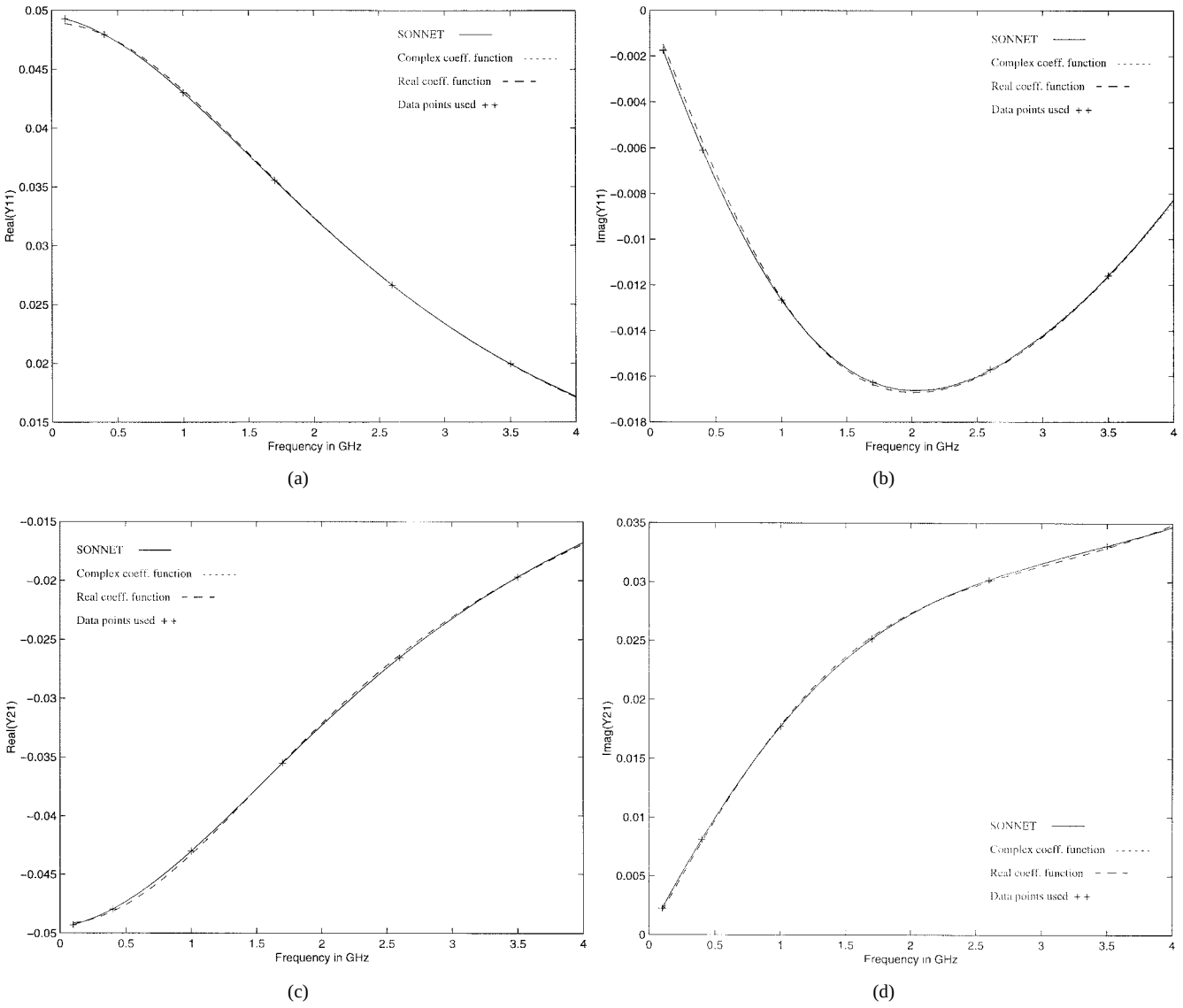

Fig. 9. Admittance parameters of 26 Ω resistor: (a) Real(Y_{11}), (b) Imag(Y_{11}), (c) Real(Y_{21}), and (d) Imag(Y_{21}).

TABLE II
RESISTOR MACROMODEL USING ADMITTANCE PARAMETER FUNCTIONS. THE COEFFICIENTS ARE DEFINED IN .PARAM SECTION

```
.macro nport2 1 2 reference
g11 1 reference LAPLACE 1 reference
+ a10,a11,a12,a13 / b0,b1,b2,b3,b4
g12 1 reference LAPLACE 2 reference
+ a20,a21,a22,a23 / b0,b1,b2,b3,b4
g21 2 reference LAPLACE 1 reference
+ a20,a21,a22,a23 / b0,b1,b2,b3,b4
g22 2 reference LAPLACE 2 reference
+ a30,a31,a32,a33 / b0,b1,b2,b3,d4
.eom nport2
```

the measured TDT response, response using a simple resistor model, response using the macromodel and a DC compensated macromodel response. Small positive peaks shown in the simulation using the simple lumped resistor model is due to high impedance (>50 Ω) transition in the test vehicle. The

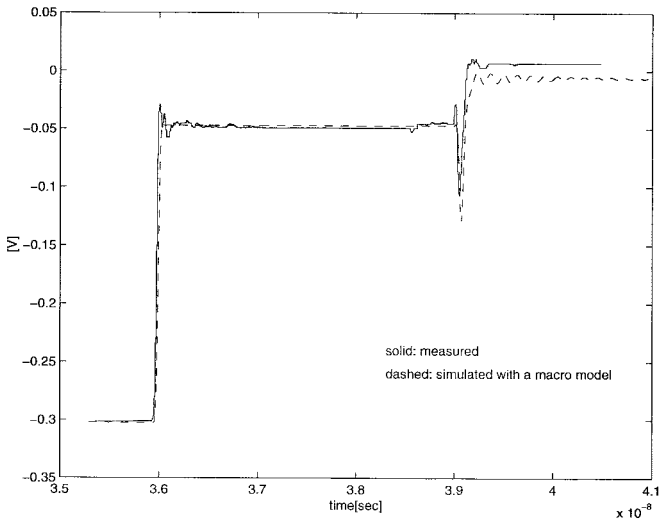

Fig. 10. TDR response of 26 Ω resistor.

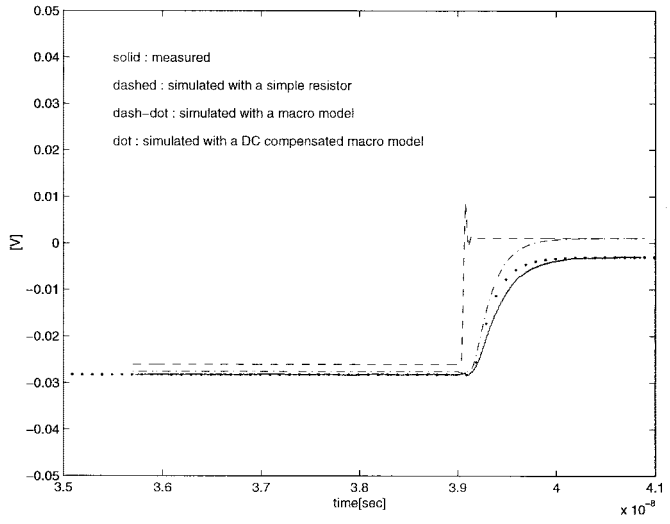

Fig. 11. TDT response of 858 Ω resistor.

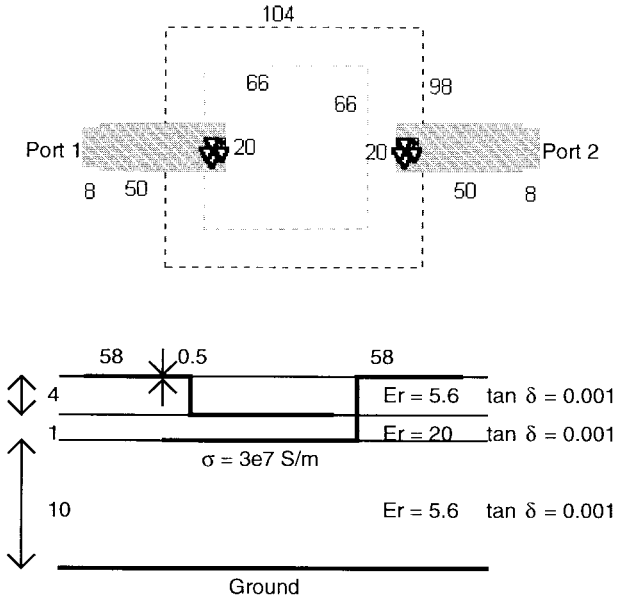

Fig. 12. Top and side view of the capacitor structure. All units are in mils.

simulations using macromodels show good agreement with measurements in all cases as compared to the simple resistor model, clearly revealing frequency dependence and parasitics. The effect of rounding of the pulse due to high frequency effects can be clearly seen in Fig. 11 for the 858 Ω resistor which has been captured accurately by the macromodel. The rounding and slanting of the pulse introduces appreciable delay at the 50% level which cannot be duplicated using a simple resistor model. The 5 mV difference in DC levels between measured values and simulated values in the TDT response can be attributed to the DC resistance of the resistor. The modeled resistance value of 858 Ω (specification) was measured to have a resistance of 868 Ω using an LCR meter. By adjusting the $a_{1,0}$, $a_{2,0}$, and $a_{3,0}$ terms in (11), the agreement between model and measurement was improved as shown in Fig. 11. This method of adjusting the low frequency coefficients of the macromodel based on measurements has been called cd compensation in Fig. 11.

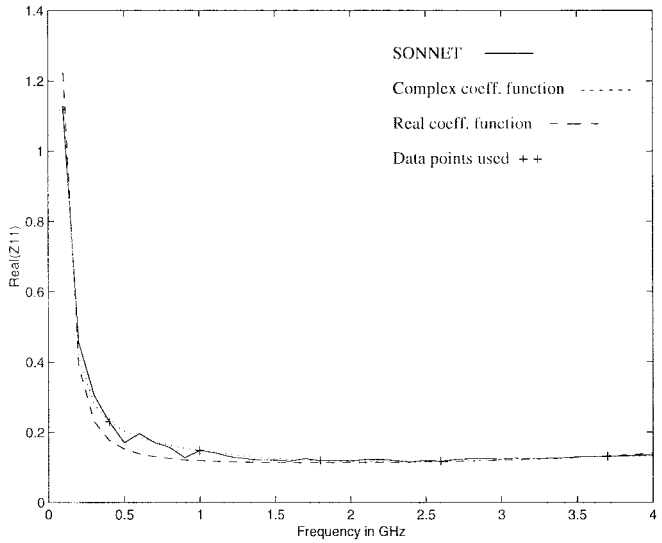

(a)

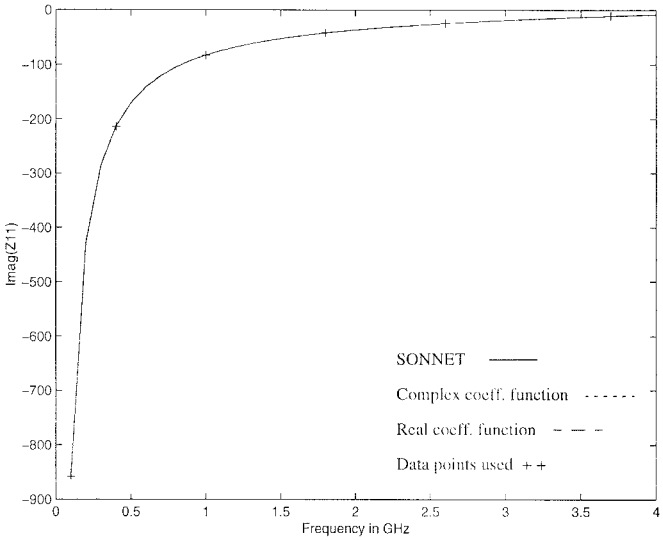

(b)

Fig. 13. Z_{11} of the capacitor: (a) Real(Z_{11}) and (b) Imag(Z_{11}).

The rational polynomial technique was next applied to a 2-port embedded capacitor. Fig. 12 shows the capacitor structure which was realized using LTCC technology. To develop the capacitor macromodel, the impedance parameters were approximated with $P = 2$ and $Q = 3$ using complex coefficients and $P = 3$ and $Q = 4$ using real coefficients. A frequency scaling factor of 10^9 was used. Fig. 13 shows the SONNET generated data and the rational polynomial response for z_{11} in the frequency range DC–4 GHz. The wiggles in SONNET data was due to convergent from "s" to "y" parameters. The TDT response of the capacitor is shown in Fig. 14. As can be seen, the macromodel agrees well with the measured TDT response indicating that all the EM effects associated with the structure have been accurately captured.

It is important to note that although the input pulse with a risetime of 35 ps has a 20 GHz bandwidth, a polynomial which provided an accurate response in the frequency range DC—4 GHz was sufficient to provide an accurate response

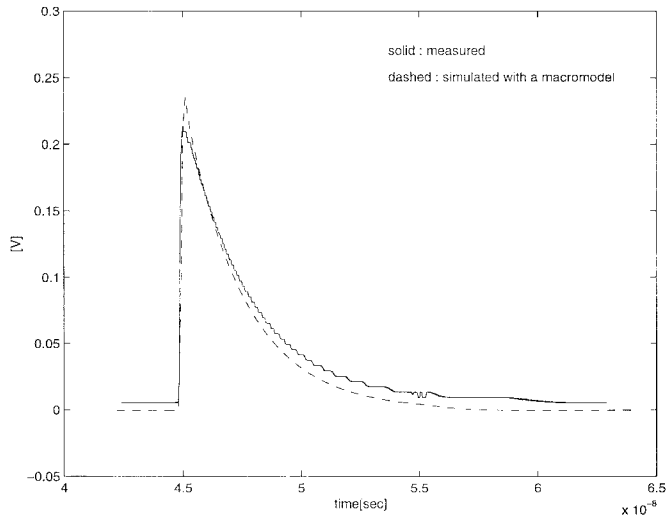

Fig. 14. TDT response of the capacitor.

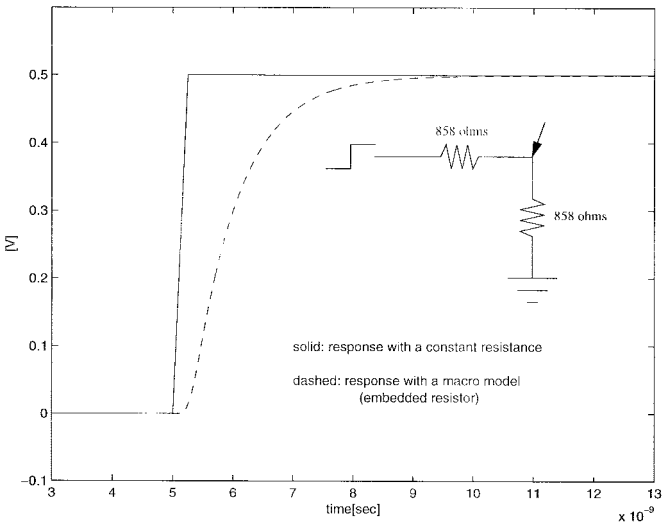

Fig. 16. Transient response of 858 Ω resistor.

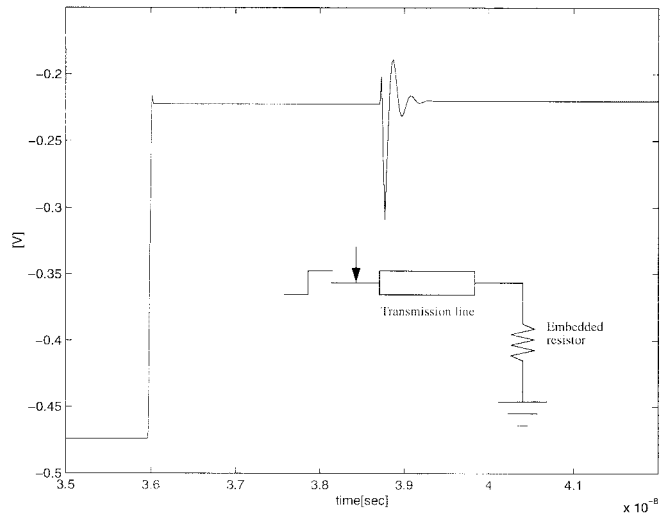

Fig. 15. Transient response of a transmission line terminated with matching impedance of embedded resistor.

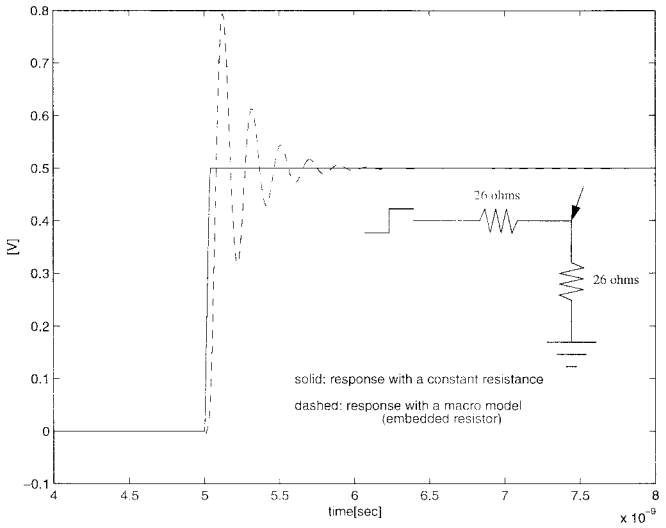

Fig. 17. Transient response of 26 Ω resistor for a step input with 35 ps rise time.

in the time domain. This greatly simplifies and reduces the analysis of such structures.

VII. Embedded Resistors in High Speed Digital Circuits

This section discusses the use of embedded resistors (as an example) in high speed digital circuits. Simple circuits have been used to elaborate the importance of parasitics and frequency dependence on the behavior of embedded resistors and similar embedded passive structures. All results in this section are based on macromodels embedded in a SPICE simulation and have been used to generate the results.

To study the effect of terminating digital transmission lines using embedded resistors, a 50 Ω transmission line terminated with a 50 Ω embedded resistor was simulated using a step with a 35 ps rise time. Due to the capacitive and inductive nature of the resistor, the ringing in the reflected response can be seen in Fig. 15 which can cause problems in high speed circuits. This ringing would be absent with an ideal resistor. Next, two voltage divider networks (typically used in analog–digital converters) using two embedded resistors and two ideal resistors were simulated using a 35 ps risetime pulse, as shown in Figs. 16 and 17. In Fig. 16, the 858 Ω resistor divider network causes a considerable slow-down of the rise time while the 26 Ω resistor network causes oscillations as shown in Fig. 17. In both Figs. 16 and 17, the response at the output is shown and is substantially different from the ideal resistor response. Hence though a simple divide-by-two voltage divider network has been used, the response is largely dependent on the physical structure and the associated parasitics. Thus considerable emphasis in designing embedded resistors is necessary for high speed circuits.

VIII. Conclusion

A macromodeling technique has been discussed in this paper for embedded passive structures. Using a minimum number of data points, the technique interpolated the data and produced a ratio of polynomials that accurately approximated the response of the embedded components in the desired

frequency domain. Suitable macromodels were created using the polynomials generated by the technique. The results showed that the interpolation technique saves a significant amount of EM simulation time in predicting the behavior of embedded passive components. The rational polynomial was suitably modified to enable transient simulation. Small order of the polynomials should also be noted, demonstrating that the response of embedded passives which are created from distributed elements can be represented using a few dominant poles and zeros. The simulated response of macromodels showed good agreement with measurements in the time domain, confirming inclusion of parasitic effects and frequency dependence in the model. Simple voltage dividing networks were simulated using macromodels to study the importance of parasitics and frequency dependence, and the results have been discussed.

ACKNOWLEDGMENT

The authors would like to thank A. Haridass, IBM, for the inductor results, A. Sood, Georgia Tech, for the capacitor measurements, and Dr. R. Adve, Rome Labs, for helpful discussions. The authors are also thankful to Dr. Y. Narayan, Dr. J. Prokop, Dr. A. Fathy, and Dr. B. Geller, Sarnoff Corporation, for their support, stimulating discussions, and fabrication of the test vehicles.

REFERENCES

[1] A. Ruehli, "Partial element equivalent circuit (PEEC) method and its application in the frequency and time domain," in *IEEE Int. Symp. Electromagn. Compat.*, 1996, pp. 128–133.
[2] SONNET User's Manual, SONNET Software, Inc., vol. 1, Sept. 1996.
[3] D. G. Swanson, "Simulating EM fields," *IEEE Spectrum*, pp. 34–37, Nov. 1991.
[4] K. L. Choi and M. Swaminathan, "Utilization of fast algorithm to analyze embedded passive components using commercial EM solvers," in *IEEE 6th Topical Meeting Elect. Perf. Electron. Packag.*, Oct. 1997, pp. 240–243.
[5] K. Kottapalli, T. Sarkar, Y. Hua, E. Miller, and G. Burke, "Accurate computation of wide-band response of electromagnetic systems utilizing narrow-band information," *IEEE Trans. Microwave Theory Tech.*, vol. 39, pp. 682–688, Apr. 1991.
[6] R. Adve, T. Sarkar, S. Rao, E. Miller, and D. Pflug, "Application of the Cauchy method for extrapolating/interpolating narrow-band system responses," *IEEE Trans. Microwave Theory Tech.*, vol. 45, pp. 837–845, May 1997.
[7] C. Huang, M. Celik, and J. L. Prince, "Simultaneous switching noise simulation for thin film packages using macromodeling technique," in *Proc. Electron. Comp. Technol. Conf.*, 1996, pp. 747–751.
[8] A. Cangellaris and J. Prince, "Modeling and simulation for mixed-signal package design," *Adv. Electron. Packag.*, vol. 19, no. 1, pp. 497–507, 1997.
[9] V. Raghavan, R. A. Rohrer, L. T. Pillage, J. Y. Lee, J. E. Bracken, and M. M. Alaybeyi, "AWE-inspired," in *Proc. IEEE 1993 Custom Integrated Circuits Conf.*, 1993, pp. 18.1.1–18.1.8.
[10] N. Na, K. L. Choi, and M. Swaminathan, "Characterization of embedded resistors for high frequency wireless applications," in *IEEE Radio Wireless Conf.*, Colorado Springs, CO, Aug. 1998.
[11] A. Sood, K. L. Choi, A. Haridass, N. Na, and M. Swaminathan, "Modeling and mixed signal simulation of embedded passive components in high performance packages," in *Proc. MCM'98 Conf.*, Denver, CO, Apr. 1998, pp. 506–511.

Kwang Lim Choi received the B.E.E. and M.S.E.E. degrees from the Georgia Institute of Technology, Atlanta, in 1995 and 1997, respectively, and is currently pursuing the Ph.D. degree in electrical engineering.

He has worked with the Packaging Research Center, Georgia Institute of Technology, since 1997. His research is focused on developing fast algorithms to allow speed-up in predicting the behavior of embedded passive components. Other research works include mixed signal simulation and synthesis of equivalent circuits of embedded passives.

Nanju Na received the B.S. degree from Kwangwoon University, Korea, in 1987, the M.S. degree from the Korea Advanced Institute of Science and Technology, in 1993, and is currently pursuing the Ph.D. degree in electrical and computer engineering at the Georgia Institute of Technology, Atlanta.

She worked for the Korea Atomic Energy Institute from 1987 to 1997. She has worked with the Packaging Research Center, Georgia Institute of Technology, since 1997, focusing on characterization of embedded passives and noise modeling in electronic packages. Her recent research interest is in characterization of simultaneous switching noise in package boards.

Madhavan Swaminathan (A'91–M'95) received the B.E. degree in electronics and communication from the Regional Engineering College, Tiruchi, India, in 1985 and the M.S.E.E. and Ph.D. degrees in electrical engineering from Syracuse University, Syracuse, NY, in 1989 and 1991, respectively.

He is an Associate Professor with the School of Electrical and Computer Engineering, Group Leader for the Systems Prototyping, Design, and Test Group, and Director of Infrastructure, at the Packaging Research Center, Georgia Institute of Technology, Atlanta. During his graduate study, he was involved in the numerical modeling of waveguides, antennas, and transmission lines for microwave applications and their implementation on parallel computers. In 1990, he joined the Advanced Technology Division, Packaging Laboratory, IBM, East Fishkill, NY, where he was involved with the design, analysis, measurement and characterization of packages for high performance systems, and low-cost multilayer thin film technology. He joined the Packaging Research Center in 1994 to pursue unique challenges arising in low-cost packaging for computer, telecommunication, and consumer applications. He has over 50 publications in refereed journals and conferences, five issued patents, and three patents pending.

Dr. Swaminathan received the Northeast Parallel Architecture Center Fellowship for his work on the solution of large matrix problems on parallel computers. He is the Co-Chair for the Topical Meeting on Electrical Performance of Electronic Packaging. He is the co-founder of the Next Generation IC and Package Design Workshop for which he is the General Chair.